Control of Separated Flows over Membrane Wings using Adaptive Membrane Compliance

Jillian Bohnker[1,2*] and Kenneth Breuer[1]

[1] Brown University, School of Engineering, Providence, RI, USA

[2] Naval Undersea Warfare Center, Newport, RI, USA

[*] jillian_bohnker@brown.edu

Abstract

Membrane wings are known to exhibit desirable aerodynamic performance in low Reynolds number flows, in part because they can passively adapt to flow conditions, delaying stall to significantly higher angles of attack. Rigid wings, on the other hand, often rely on active flow control mechanisms to maintain attached flow at high angles of attack, injecting momentum to induce or strengthen vortex roll-up in the separating shear layer. Here, we demonstrate successful active flow control with a membrane wing comprised of a dielectric elastomer which is actuated so that it can dynamically change its compliance. The performance of a sinusoidally-actuated membrane wing is characterized for a range of actuation frequencies, freestream velocities, and angles of attack. Force measurements show lift enhancement of up to 20%. Dynamic mode decomposition is used to identify vortical structures being shed from the leading edge in phase with the actuation. The effect of actuation frequency, the location of shear layer, and fluid-induced damping are also discussed.

1 Introduction

A rich body of literature reports on techniques to control the flow that has separated from a thin wing at high angles of attack (e.g. Greenblatt and Wygnanski, 2000; Glezer et al., 2005)). Techniques range from steady suction or blowing to unsteady methods, which utilize acoustic pressure waves, synthetic jet or plasma actuators. However, these techniques are difficult or impossible to implement on membrane wings.

Compliant membrane wings are known to have excellent aerodynamic performance at low Reynolds numbers (Song et al., 2008; Waldman and Breuer, 2017), achieved by passively adapting to the flow conditions. Although compliance allows the wing to delay stall to significantly higher angles of attack (relative to rigid wings or inextensible membrane wings), little can be done to reattach or control the flow following separation. In this work, an approach to effective control is described.

A dielectric elastomer actuator (DEA) may be used as the lifting surface for a low aspect ratio membrane wing. Applying a voltage relaxes the membrane tension, thus allowing the camber to be dynamically adjusted. Both DC (Hays et al., 2012) and AC (Curet et al., 2014) excitation have shown improvements in aerodynamic performance, although the flow mechanisms behind the changes are still unclear. In this paper, the performance of unsteadily-actuated dielectric elastomer membrane wings will be examined in further detail. Particle image velocimetry (PIV) flow field analysis is combined with 3D time-resolved membrane kinematics to understand the fluid-structure interactions, and lift/drag data is analyzed for actuated and un-actuated wings.

2 Experimental Methods

The membrane wing was constructed from a rigid acrylic frame ($180{\times}90{\times}3.175$ mm^3), with two symmetric openings ($76{\times}76$ mm^2) for the membrane. The membrane was an acrylic elastomer (VHB4905, 3M), prestrained to 250%, with carbon powder electrodes applied to both top and bottom surfaces, using the membrane's adhesive properties. The membrane was attached to the acrylic frame, creating a rectangular

Table 1: Summary of data collected. Dataset I includes time-resolved and synced PIV, membrane kinematics, and aerodynamic forces and torques. Dataset II includes only forces and torques.

	Velocity (m/s)		Angle of attack (°)		Frequency (Hz)	
	Range	Increment	Range	Increment	Range	Increment
Dataset I	10-20	5	15-30	5	50, 75, 115	N/A
Dataset II	5-25	2	10-40	5	10-300	10

membrane wing with full perimeter support. The dielectric membrane actuator was actuated using a high-voltage amplifier (Trek, model 5-80, Lockport, NY) and a sinusoidal input, $V(t) = V_0(1 + \sin 2\pi f_{act}t)$. The actuation voltage, V_0, was kept constant at 2 kV and the frequency, f_{act}, ranged from 10 to 300 Hz.

The wing was tested in a temperature-controlled closed-loop wind tunnel (Figure 1) at Brown University, with a test section measuring 0.61 m × 0.61 m in cross-section, and 1.22 m in length. The wing was placed approximately in the center of the test section mounted onto a rigid fairing, and held at the desired angle of attack with a custom-machined adapter. Freestream velocities ranged from 5 m/s to 25 m/s, and angle of attack was varied from 10° to 40°. A six-axis load cell (F/T Nano17, ATI Industrial Automation, Apex, NC) was positioned between the angle of attack adapter and the wing, at quarter-chord, and used to measure the aerodynamic forces and torques. Aerodynamic forces and torques were recorded at 2 kHz. For each testing configuration, 20 seconds of data was recorded without actuation, followed immediately by 30 seconds of data collection with the actuation in operation. In addition to aerodynamic load measurements, time-resolved 2D-2C PIV and 3D membrane kinematics were collected for a subset of experimental conditions, as detailed in Table 1.

Two series of measurements were conducted. In the first series, time-resolved and synchronized PIV, membrane kinematics, and aerodynamic forces and torques were acquired using a membrane under 250% pre-stretch. A range of freestream velocities, angles of attack, and actuation frequencies (Dataset I, Table 1) provided a detailed picture of the flow field and the aerodynamic coefficients, as well as their phase-locked relationship to the membrane motion. A second series of measurements was also conducted, recording only the aerodynamic coefficients, but over a wider range of actuation frequencies and freestream velocities (Dataset II, Table 1).

3   Results and Discussion

The lift enhancement produced by the described actuation can be seen to be a function of angle of attack, freestream velocity, and frequency, as shown in Figure 2. Within this range of actuation frequencies (50-115 Hz), significant lift enhancement is consistently seen in the range of 7-15 m/s freestream velocity and between 15° and 30° angles of attack. A number of factors go into establishing this range. The influence of actuation frequency, shear layer susceptibility, shear layer location, and fluid induced damping will be considered. These factors will be considered as a function of both reduced frequency, $f^+ = f_{act}c/U_\infty$, and aeroelastic number, $Ae = Eh/0.5\rho U_\infty^2 c$, where E is the membrane modulus, h is the membrane thickness, and ρ is the membrane density.
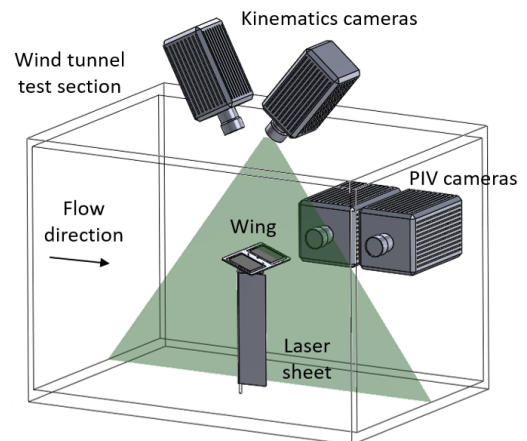

Figure 1: Experimental set-up. Aerodynamic forces and torques are measured with a six-axis load cell, time-resolved membrane kinematics are measured with two high-speed cameras, and the flow field is captured with a PIV laser sheet and two high-speed cameras. The membrane wing is fixed in the center of the wind tunnel cross-section with a rigid fairing and an angle of attack adapter.
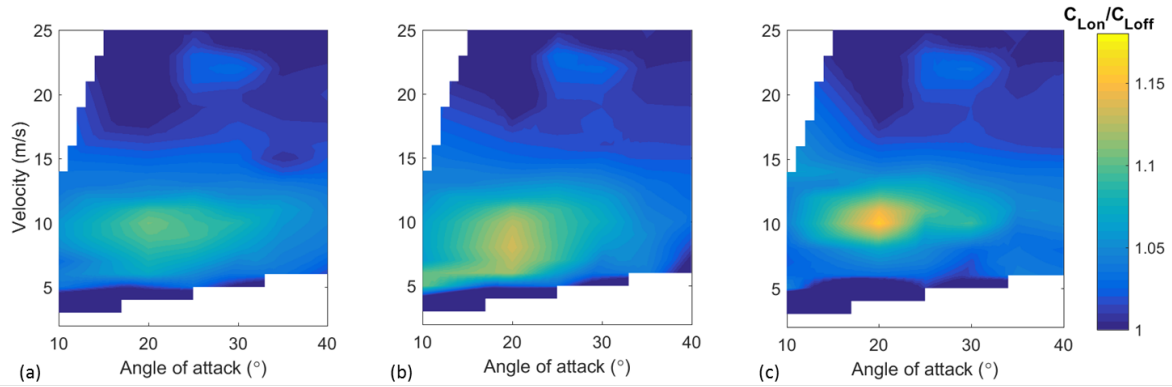
Figure 2: The lift enhancement, relative to an unactuated wing in the same conditions, is shown as a function of angle of attack and freestream velocity for a wing being actuated at (a) 50 Hz, (b) 75 Hz, and (c) 115 Hz.

Because this method of flow control is thought to rely on the excitation of the global bluff-body vortex shedding instability and/or the local shear layer roll-up instability (Wu et al., 1998), the frequency of actuation plays a significant role in successfully enhancing lift, as shown in Figure 3. Here, the lift enhancement is plotted as a function of reduced frequency for several angles of attack and freestream velocities. Angle of attack and freestream velocity are seen to have some effect, such that a wing at 25° exhibits a broader range of optimal reduced frequencies relative to a wing at 30°, and the amplitude of lift enhancement is generally higher for lower freestream velocities. Despite these differences, the effect of reduced frequency remains fairly consistent, resulting in optimum lift enhancement between reduced frequencies of 0.5-1. This is consistent with synthetic

Figure 3: The effect of actuation frequency on the coefficient of lift is shown, where $f^+ = f_{act}c/U$, for wings at 25° and 30° and 10-15 m/s.

jets being operated at $f^+ \sim O(1)$ (Greenblatt and Wygnanski, 2000), though effective operation can also occur at $f^+ \sim O(10)$ and higher (Glezer et al., 2005) through different mechanisms.
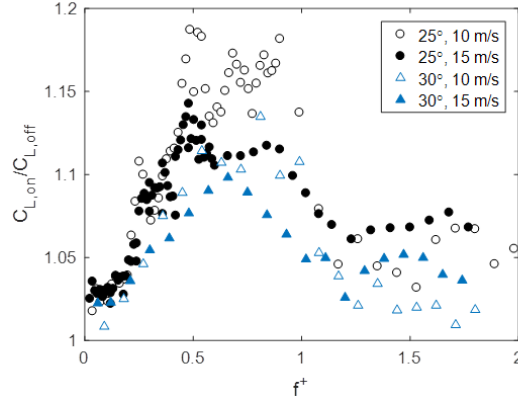
The physical cause of this optimum range of actuation frequencies can be seen using dynamic mode decomposition (Schmid, 2010). This method decomposes time-resolved data into modes, each of which has a single characteristic frequency. The eigenvalue analysis acts to approximate a linear operator that best captures the dynamics of the flow (Taira et al., 2017). In Figure 4, modes are calculated from the vorticity field in the region immediately downstream of the leading edge of the wing, and the mode corresponding with the frequency of actuation is selected. A variety of Ae and f^+ values are shown, with (a-c) showing modes with $U_\infty = 10$ m/s, $Ae = 3.7$ and (d-f) showing $U_\infty = 15$ m/s, $Ae = 1.6$, at reduced frequencies ranging from 0.114 to 1.348. It is seen that at low reduced frequencies, where lift enhancement is negligible (Figure 3), there are no coherent structures seen at the actuation frequency (Figure 4a). However, as the reduced frequency increases, lift enhancement is observed, and coherent vortical structures are seen in the region of the separated shear layer (Figure 4b,d,e). At a reduced frequency of 0.449, only a single pair of vortices are seen over the chord of the wing, and as the reduced frequency increases further, the vortices become more closely packed. Finally, as the reduced frequency is increased to 1.348, DMD continues to identify vortices in the shear layer, though lift enhancement is very small. Because DMD is an eigenvalue analysis, the real value of the mode's eigenvalue can be used to estimate the mode's growth factor. Considering the growth factor as a function of reduced frequency (Figure 4g), it is seen that the growth factor becomes negative at this high reduced frequency, indicating that the vortices seen in the high reduced frequency mode are damped and do not grow in time.
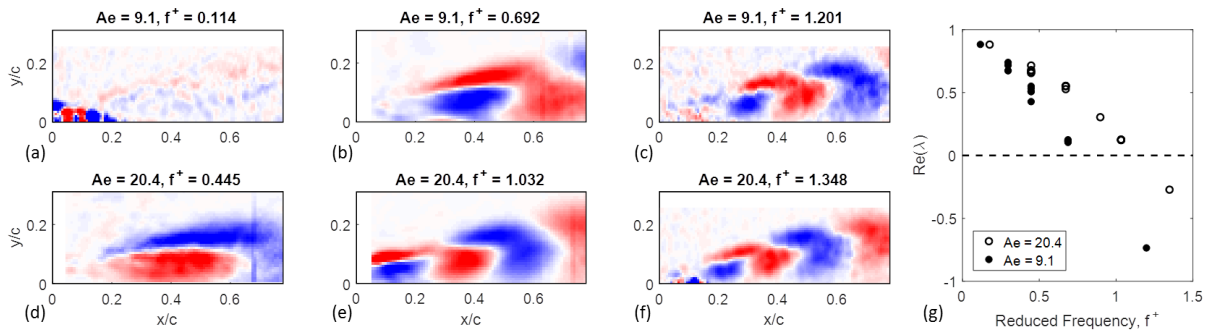
Figure 4: The DMD mode at the frequency of actuation is shown for the region immediately behind the leading edge of the wing for a range of Ae and f^+ conditions (a-f). In (g), the real part of the mode's eigenvalue is plotted against reduced frequency, suggesting that at high reduced frequency, the real portion of the eigenvalue is negative and the mode is temporally damped.
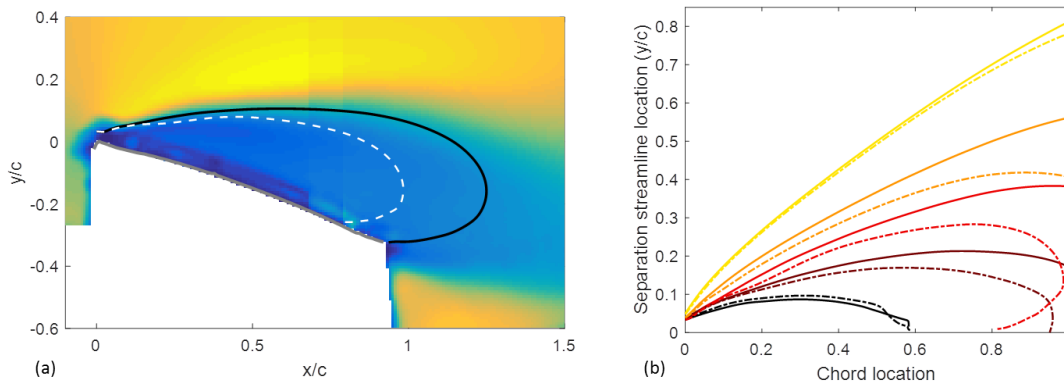

Figure 5: (a) An example time-averaged flow field at 20° and 10 m/s freestream velocity is shown, with the separation streamline of an unactuated wing (black solid) and a 50 Hz actuated wing (white dashed) shown, where the separation streamline is defined as the streamline passing through a point 2 mm above the leading edge of the wing. (b) The relative location of the separation streamlines for unactuated wings (solid lines) and actuated wings (dashed lines) for a range of angles of attack from 10° to 30°, with 50 Hz actuation and 10 m/s freestream velocity.

For successful flow control, in addition to exciting the shear layer at an appropriate reduced frequency, the shear layer location must be such that it is susceptible to excitation. In Figure 5a, the time-averaged unactuated flow field at 20° and 10 m/s is shown, with the location of the separation shear layers for the unactuated (solid black line) and the actuated flow (dotted white line) superimposed. The shear layer location is (arbitrarily) defined by the streamline passing through the point located two millimeters above the leading edge. In Figure 5b, the location of this streamline is shown for all unactuated (solid lines) and actuated (dotted lines) flows with angles of attack from 10° to 30°. It can be seen that the separation streamlines are significantly affected by membrane actuation for angles of attack between 15° and 25°, such that the separation bubble is reduced in size. At 10°, the separation is minimal, and actuation has little to no effect on the separation streamline. At 30°, the flow is so massively separated that the separation streamline has moved quite far from the surface of the wing. In this case, the effect of actuation is also minimal, presumably because the shear layer is too far from the surface of the wing to be effectively controlled.

In addition to the factors already discussed, the amplitude of membrane motion during actuation must be sufficient to affect the instability. One complicating factor in achieving effective actuation is fluid-induced damping, which can be estimated here with a simple pseudo-static aeroelastic analysis, valid for intermediate values of reduced velocity ($U_R = U_\infty / f_{act} c$) (Païdoussis et al., 2010), equivalent to the inverse of the reduced frequency. The reduced velocity varies from 0.97 to 4.44 for the conditions tested in Dataset I (Table 1). For these intermediate values, fluid-induced stiffness (k) is proportional to the inverse aeroelastic number (Ae),
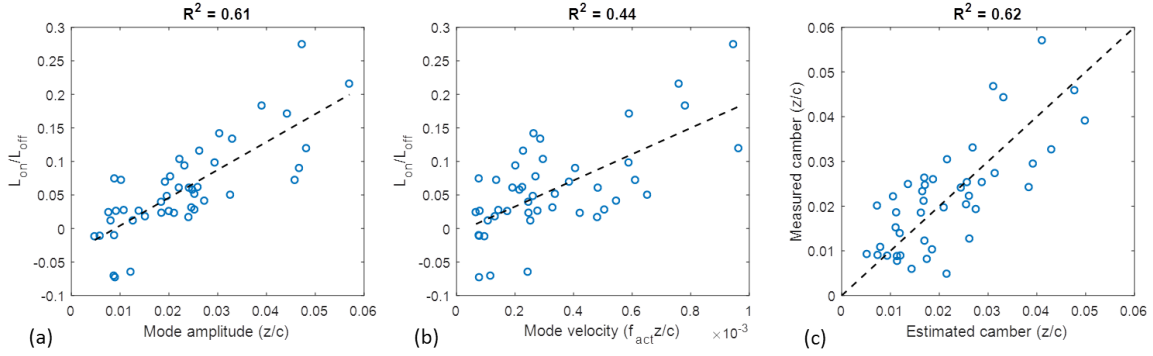
Figure 6: The relationship between (a) mode amplitude and enhanced lift and (b) mode velocity and enhanced lift, shown for the parameter range investigated in Dataset I (Table 1). (c) The resulting predicted amplitude of vibration, compared with the measured amplitude of camber variation during actuation, suggests flow-induced stiffness and damping are significant. Stiffness and damping are approximated with a pseudo-static aeroelastic analysis, and the driven harmonic oscillator equation is solved.

as well as the sensitivity of the coefficient of lift to the vibration amplitude, $\tilde{z}e^{j\omega t} = z/c$, (Païdoussis et al., 2010). Similarly, the fluid-induced damping (b) is proportional to the inverse aeroelastic number (Ae) and the sensitivity of the lift coefficient to the vibration velocity ($f_{act}\tilde{z}$) on the coefficient of lift:

$$k = Ae^{-1}\frac{\partial C_L}{\partial \tilde{z}}, \quad \text{and} \quad b = Ae^{-1}\frac{\partial C_L}{\partial(f_{act}\tilde{z})}. \tag{1}$$

To estimate k and b, the relative affect of the membrane motion on the coefficient of lift must be estimated. To do this, we consider the experimental relationship between the amplitude of phase-averaged C_L and $\tilde{z}$, shown in Figure 6(a-b) for all conditions tested in Dataset I. A reasonably good correlation is seen between enhanced lift and vibration amplitude ($\partial C_L/\partial \tilde{z}$), as well as between enhanced lift and vibration velocity ($\partial C_L/\partial(f_{act}\tilde{z})$). Applying a linear regression to the data, the partial derivatives in equation 1 can be estimated to have values of 4.58 and 215, respectively.

Using these results, the expected amplitude of membrane motion can be estimated by the standard equations of a driven damped harmonic oscillator (Kinsler et al., 1999):

$$Fe^{j\omega t} = m\frac{d^2z}{dt^2} + b\frac{dz}{dt} + kz, \tag{2}$$

where m is the mass of the membrane and $Fe^{j\omega t}$ is the complex driving force of the oscillator. Solving for the complex displacement,

$$z = \frac{1}{j\omega}\frac{Fe^{j\omega t}}{b + j(\omega m - k/\omega)} = \frac{1}{j\omega}\frac{Fe^{j\omega t}}{Z_m}, \tag{3}$$

where Z_m is the complex mechanical impedance. The amplitude of the displacement is given by the magnitude of the real part of Equation 3.

Calculating Z_m from the stiffness and damping coefficients derived from Figure 6(a-b) and using an arbitrary value of F, the expected amplitude of motion can be estimated and compared to the actual amplitude of camber variation during actuation, as shown in Figure 6c. Though significant scatter is seen, the experimental phase-averaged camber is seen to follow the same trend as the vibration amplitude predicted by a driven damped oscillator. The comparison is limited by the approximate nature of the estimate of $\partial C_L/\partial \tilde{z}$, which is certainly dependent on other parameters, most notably the reduced frequency. Indeed, the R^2 values at each fit, ranging from 0.44 to 0.62, suggest that the dynamics are not fully captured by the aeroelastic number alone. However, the trend of reduced performance at high freestream velocities is consistent with fluid-induced loading.

4 Conclusions

Successful lift enhancement has been shown to be driven by instabilities in the separated flow, requiring excitation within a range of susceptible reduced frequencies. The shear layer must be separated and located sufficiently near the membrane to be affected by the actuation. Additionally, the excitation of instabilities is impossible when the actuation mechanism is insufficient to overcome the fluid-induced damping of the system. Therefore, flow control using a membrane wing requires careful attention to both f^+ and Ae for optimal performance.

The development of active flow control techniques for membrane wings will become increasingly important with the ongoing development of micro air vehicles (MAVs). Integrated active flow control, as demonstrated here with dielectric elastomer actuator membranes, will enable MAVs to operate in a wider range of flow conditions, respond to flow unsteadiness, and improve maneuverability. In this work, a possible mechanism for active flow control of membrane wings is presented and contributing factors to control effectiveness are discussed. The initial results are promising, resulting in lift enhancements of up to 20% over a range of experimental parameters.

Acknowledgements

References

Curet OM, Carrere A, Waldman R, and Breuer KS (2014) Aerodynamic Characterization of a Wing Membrane with Variable Compliance. *AIAA Journal* 52:1749–1756

Glezer A, Amitay M, and Honohan AM (2005) Aspects of Low- and High-Frequency Actuation for Aerodynamic Flow Control. *AIAA Journal* 43:1501–1511

Greenblatt D and Wygnanski IJ (2000) Control of Flow Separation by Periodic Excitation. *Progress in Aerospace Sciences* 36:487–545

Hays MR, Morton J, Dickinson B, and Uttam K (2012) Aerodynamic Control of Micro Air Vehicle Wings using Electroactive Membranes. *Journal of Intelligent Material Systems and Structures* 24:862–878

Kinsler LE, Frey AR, Coppens AB, and Sanders JV (1999) *Fundamentals of Acoustics*. Wiley

Païdoussis MP, Price SJ, and De Langre E (2010) *Fluid-Structure Interactions: Cross-Flow-Induced Instabilities*. Cambridge University Press

Schmid PJ (2010) Dynamic mode decomposition of numerical and experimental data. *Journal of Fluid Mechanics* 656:5–28

Song A, Tian X, Israeli E, Galvao R, Bishop K, Swartz S, and Breuer K (2008) Aeromechanics of Membrane Wings with Implications for Animal Flight. *AIAA Journal* 46:2096–2106

Taira K, Brunton SL, Dawson ST, Rowley CW, Colonius T, McKeon BJ, Schmidt OT, Gordeyev S, Theofilis V, and Ukeiley LS (2017) Modal analysis of fluid flows: An overview. *AIAA Journal* pages 1–29

Waldman RM and Breuer KS (2017) Camber and Aerodynamic Performance of Compliant Membrane Wings. *Journal of Fluids and Structures* 68:390–402

Wu JZ, Lu XY, Denny AG, Fan M, and Wu JM (1998) Post-Stall Flow Control on an Airfoil by Local Unsteady Forcing. *Journal of Fluid Mechanics* 371:21–58